

Cages and anomalous diffusion in vibrated dense granular media

Camille Scalliet

*Université de Lyon, Ecole Normale Supérieure de Lyon,
Laboratoire de physique, 46 Allée d'Italie, 69364 Lyon, Cedex 07, France and
Dipartimento di Fisica, Università "Sapienza", Piazzale Aldo Moro 5, 00185 Rome, Italy*

Andrea Gnoli and Andrea Puglisi

*Istituto dei Sistemi Complessi - Consiglio Nazionale delle Ricerche, Rome, Italy and
Dipartimento di Fisica, Università "Sapienza", Piazzale Aldo Moro 5, 00185 Rome, Italy*

Angelo Vulpiani

*Dipartimento di Fisica, Università "Sapienza", Piazzale Aldo Moro 5, 00185 Rome, Italy and
Istituto dei Sistemi Complessi - Consiglio Nazionale delle Ricerche, Rome, Italy*

A vertically shaken granular medium hosts a blade rotating around a fixed vertical axis, which acts as a mesorheological probe. At high densities, independently from the shaking intensity, the blade's dynamics show strong caging effects, marked by transient sub-diffusion and a maximum in the velocity power density spectrum (vpds), at a resonant frequency ~ 10 Hz. Interpreting the data through a diffusing harmonic cage model allows us to retrieve the elastic constant of the granular medium and its collective diffusion coefficient. For high frequencies f , a tail $\sim 1/f$ in the vpds reveals non-trivial correlations in the intra-cage micro-dynamics. At very long times (larger than 10 s), a super-diffusive behavior emerges, ballistic in the most extreme cases. Consistently, the distribution of slow velocity inversion times τ displays a power-law decay, likely due to persistent collective fluctuations of the host medium.

PACS numbers: 45.70.-n, 05.40.-a, 47.57.Gc

A comprehensive theory of dense granular media is still lacking [1]. Unperturbed granular systems may support external forces without flowing, behaving like a solid: in this configuration, a granular packing may show an elastic response to small stresses. Under gentle tapping, the granular medium undergoes very slow rearrangements, which resemble the sluggish response of molecular glasses [2–5]. The jamming transition, observed when reducing the vibration intensity, or increasing the density, is commonly compared to the glass transition in under-cooled liquids [6]. When the energy of the external vibration is increased or the density is decreased, the granular medium enters a liquid-like phase [7] which has not received as much amount of attention as the glass/solid phases or the much more dilute gas phase [8]. Nevertheless, learning from molecular fluids, the dynamics of the liquid phase is rich of information: in particular, it gives important hints about the many timescales developing when the glass transition is approached from above [9]. Recent theoretical and experimental insights in the liquid phase have highlighted the differences between molecular glass-formers and driven granular media, in particular the presence of superdiffusive behavior [10–13].

As rheometers are usually conceived to apply the excitation at the boundaries, standard rheology in granular liquids is typically limited by problems of slip and shear localization. Other techniques exist to probe the bulk response properties of granular media, e.g. magnetic resonance imaging, X-ray tomography and high-speed particle tracking [14], confocal microscopy [15] or multispeckle

dynamic light scattering [11]. Microrheology [16] is also used, e.g. to probe transient subdiffusive behavior and cage effects [17]. However, it is not evident the ability of small intruders to probe the collective behavior at large spatial scales in the host granular medium.

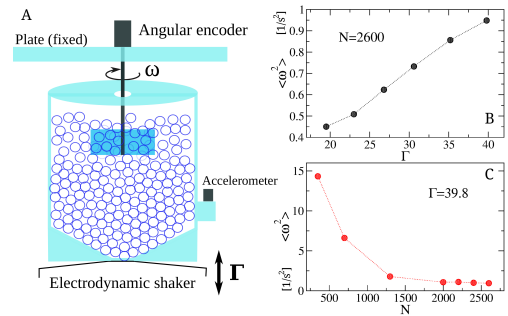


FIG. 1: A: Schematic of the experimental setup. B and C: mean squared angular velocity of the blade in the various experiments.

We propose a technique which could be named passive *mesorheology*, see Fig. 1A, inspired from previous works [7, 18–20]. The granular medium made of spheres of diameter $d = 4$ mm is placed in a cylindrical container of volume ~ 7300 times that of a sphere. The container is vertically shaken with a signal whose spectrum is approximately flat in a range $[f_{min}, f_{max}]$ with $f_{min} = 200$ Hz and $f_{max} = 400$ Hz. A blade, our probe with cross section $\sim 8d \times 4d$, is suspended into the granular medium and rotates around a vertical axis. Its angular velocity

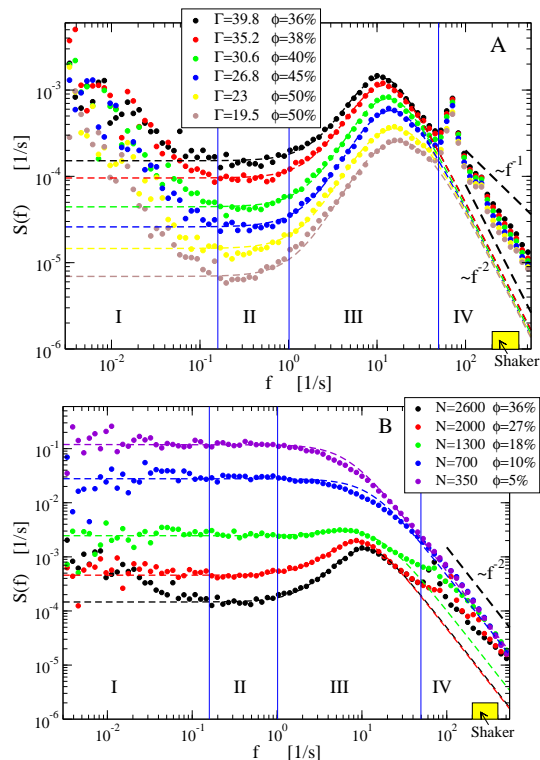


FIG. 2: Power density spectra of the blade’s angular velocity for the two series. A: the number of beads is fixed ($N = 2600$) and the shaking intensity varies. B: the shaking intensity is fixed to $\Gamma = 39.8$ and N changes. The frequencies of vibration are marked by the yellow bar. Dashed lines are fits to the Eq. (2) to the experimental data in regions II and III. Thick-dashed lines show the limit behaviors f^{-2} and f^{-1} .

$\omega(t)$ and the traveled angle of rotation $\theta(t) = \int_0^t \omega(t') dt'$ are measured with a time-resolution of 2 kHz. The blade, interacting with the spheres, performs a motion qualitatively similar to an angular Brownian motion. Two families of experiments have been performed: a) a series at high density ($N = 2600$), varying the shaking intensity $\Gamma = \ddot{z}_{max}/g \in [19.5, 39.8]$, and b) a series at high shaking intensity ($\Gamma = 39.8$), varying $N \in [300, 2600]$ and the packing fraction ϕ as indicated in the Figures. Fig. 1B and C report the values of the mean squared angular velocity $\langle \omega^2 \rangle$ of the blade in the different experiments. Details on dimensions of the setup and shaken parameters are reported in Supplemental Material [21].

Velocity power density spectrum (vpds): in Fig. 2, we present our main results in the form of the power density spectrum of the velocity signal $\omega(t)$, which is defined as $S(f) = \frac{1}{2\pi t_{TOT}} |\int_0^{t_{TOT}} \omega(t) e^{i(2\pi f)t} dt|^2$. We recognize 4 frequency ranges, denoted as regions I, II, III and IV. In the experiments at fixed (maximum) density, $N = 2600$, displayed in Fig. 2A, the spectrum conserves the same qualitative shape, vertically shifted due to the differences in Γ . The most striking properties are observed in regions II and III: $S(f)$ goes from a plateau in region II

to a roughly parabolic maximum centered at a frequency f^* in region III. The value of the resonant frequency f^* slightly shifts from 10 Hz to 20 Hz as Γ decreases. To avoid interference, we ensured that the shaker vibration is in a distant region (200 – 400 Hz); we changed such a range (including trials with a single frequency, i.e. a harmonic vibration), obtaining always the same shape $S(f)$ with same values of f^* . A mechanical resonance is also observed at ~ 70 Hz, due to the non-perfect acoustic insulation of the plate on which the couple encoder/blade is mounted. In conclusion, the maximum in f^* is a resonance experienced by the blade in its motion through the granular medium, and we interpret it as a transient trapping phenomenon, analogous to caging effects in low-temperature/high-density liquids. We will see that such an interpretation is well supported by other observations and by a theoretical model. In both “extremal” regions I and IV, $S(f)$ is a decreasing function of f . In particular, in region IV, the high-frequency decay presents a power law $\sim f^{-\beta}$ with $1 < \beta < 2$, close to 1 for the lowest values of Γ . This is the evidence of collective effects, in the fast processes *inside a cage* (as $f \gg f^*$), occurring without a characteristic frequency [22]. The decay in region I is also anomalous and denotes the emergence of long characteristic times, possibly larger than the experiment duration $t_{TOT} = 3600$ s. Note that the asymptotic diffusion is governed by $\lim_{t \rightarrow \infty} \langle \Delta \theta^2(t) \rangle / t \sim 2\pi S(f \rightarrow 0)$: therefore an increasing value of $S(f)$ as $f \rightarrow 0$ (i.e. at increasing time) indicates a superdiffusive behavior, detailed below.

When the density is reduced, see Fig. 2B, the shape of $S(f)$ drastically changes. The slope of the decay in region I decreases and eventually vanishes: at low densities a plateau spans both regions I and II. The maximum in region III is reduced and disappears for $N < 1000$, called the “gas”-phase. The exponent of the power-law decay in region IV increases $\beta \rightarrow 2$. The whole spectrum at the lowest densities is well fit by the Lorentzian $S(f) = \frac{T}{\pi\gamma} / [1 + (2\pi I f / \gamma)^2]$, expected for diffusion in diluted gases at temperature T with a collision frequency $\propto \gamma$ [23]. Here T is the probe’s “kinetic temperature” $T = I \langle \omega^2 \rangle$.

Mean-square-displacement (msd). The several phenomena observed in $S(f)$ are reflected in the diffusion properties, see Fig. 3, where the mean-square displacement $\langle [\Delta \theta(t)]^2 \rangle$ after a time t is plotted. The four temporal regions corresponding to the frequency regions discussed above are marked on the graph. Our “cage-like” interpretation of the maximum of $S(f)$ in region III is corroborated, in Fig. 3A, by the dramatic slowing-down of $\langle [\Delta \theta(t)]^2 \rangle$ in the same region [24], resembling the typical dynamical slowdown in the diffusion of tracers dispersed in viscous liquids. At small times (region IV) the usual ballistic behavior appears. More remarkable is the behavior at large times. All the experiments with $N = 2600$ present a superdiffusive range $\sim t^\alpha$ in region II, with $\alpha > 1$. For the largest values of Γ , this behavior changes to a diffusive behavior $\sim t$ in region I. On the

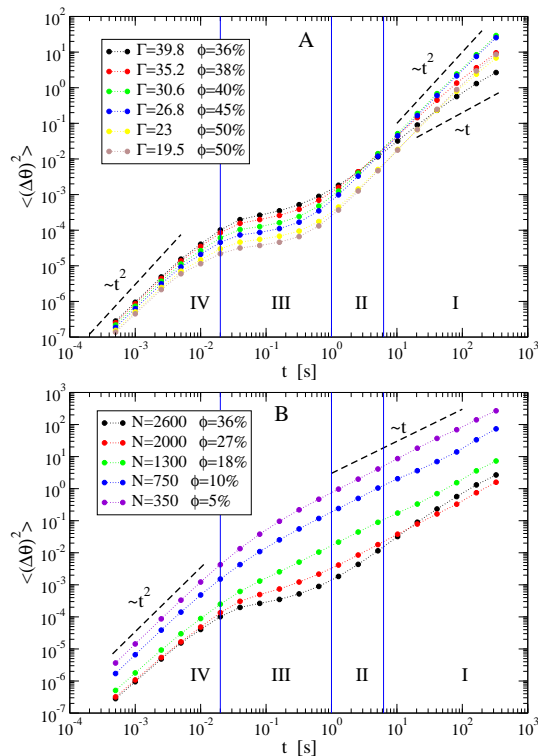


FIG. 3: Mean-squared displacement $\langle [\Delta\theta(t)]^2 \rangle$ after a time t for the two series. A: $N = 2600$ and Γ varies. B: the shaking intensity is fixed to $\Gamma=39.8$ and N changes. Black dashed lines are guides for the eye.

contrary, at lower Γ , the superdiffusive exponent $\alpha > 1$ remains the same of region II at large times. In particular, for $\Gamma < 31$, we find an almost ballistic superdiffusion $\alpha \sim 2$. The situation is very different when the density is reduced (Fig. 3B): the long time behavior (region I) is always of the normal type $\sim t$. In the most dilute cases ($N < 1000$) the typical scenario of diffusion in a gas-like fluid is fully recovered in the form of a monotonic crossover from the ballistic region IV to the normal diffusion of region II and I. Changing the size and shape of the blade, see [21], does not lead to relevant changes in the above scenario.

The study of vpds and msd are consistent with measurements of the velocity-autocorrelation function (vacf) $C(t)$, which is the inverse Fourier transform of $S(f)$. In the very dilute cases, it is close to a simple exponential decay. The most dense and “cold” experiments, on the contrary, reveal a vacf with many features: a fast, though non-exponential, decay at small times, followed by a back-scattering oscillation through negative values, interpreted as the “cage”, and finally a slow decay to zero [25]. The final decay of the vacf could also light up the origin of superdiffusion. Unfortunately at large times the vacf is exceedingly noisy. A more promising way to probe long memory effects is to measure the times of persistency, i.e. the times during which the signal remains positively

correlated. Our operative definition consists in two basic steps: 1) filter out high frequency oscillations which are not relevant for the behavior at large times of $\Delta\theta(t)$, by taking the running average $\omega_s(t) = \frac{1}{\tau} \int_t^{t+\tau} \omega(t') dt'$ over a large time $\tau \geq 1s$; and then 2) compute the statistics of the times separating two consecutive zeros of $\omega_s(t)$, which we call inversion time t_{inv} , see Fig. 4A and 4B for experimental samples of $\omega(t)$, $\omega_s(t)$ and t_{inv} . The statistics of t_{inv} is a natural measurement of long term memory of the signal. The experimental probability density (pdf) of t_{inv} is shown in Fig. 4C- 4F for a few choices of parameters and values of τ . We observe that it rapidly decays with an exponential cut-off smaller or equal than $\sim 10s$ in all cases where the msd asymptotically showed normal diffusion, signaling a finite memory of the dynamics. The cut-off apparently jumps to a much larger value in the cases where the msd displays superdiffusion: in such cases, the pdf decays to zero as a power ~ -2 or even slower. This is a fair evidence that long memory effects arise together with the observed superdiffusion. Long memory may be due to a slow rotating creeping motion of the surrounding granular medium, which acts as a coherent block and drags the blade. Such a “secondary” motion has long relaxation times due to the involved large inertia. New experiments are being designed with the aim of demonstrating this picture. We mention that longer experiments (shown in the SM [21]) still display superdiffusion that evolves in normal diffusion after many hours.

Modelling the dynamics of the blade. In the most dense and cold experiments, the vpds and the msd display an intriguing superposition of phenomena over almost 7 decades of time-scales. It seems hopeless to reduce such a complexity to a model with a simple physical interpretation. It is tempting to disentangle the two main phenomena, i.e. caging (occurring at times smaller than $10^{-1}s$) and superdiffusion (more evident at times larger than $10s$), by decomposing the dynamics into a slow and a fast component $\omega(t) = \omega_s(t) + \omega_f(t)$, with $\omega_s(t)$ defined above. Experimental data demonstrate that the standard deviation of $\omega_f(t)$ is much larger than that of ω_s and therefore dominates at short times (large frequencies). At long times (small frequencies), on the contrary, the fast dynamics averages out and $\omega_s(t)$ emerges as the leading signal. For the fast dynamics, we propose a simple interpretation of the transient caging phenomena through a “diffusing harmonic cage” (dhc) model: this is a simplified version of the Itinerant Oscillator model describing translational and rotational diffusion of particles in liquids [26, 27], and reads

$$\dot{\theta}(t) = \omega_f(t) \quad \dot{\theta}_0(t) = \sqrt{2D_0}\xi'(t) \quad (1a)$$

$$I\dot{\omega}_f(t) = -\gamma\omega_f(t) - K[\theta(t) - \theta_0(t)] + \sqrt{2\gamma T}\xi(t), \quad (1b)$$

where $\xi(t)$ and $\xi'(t)$ are white normal Gaussian noises. The model represents the diffusion of a particle in a har-

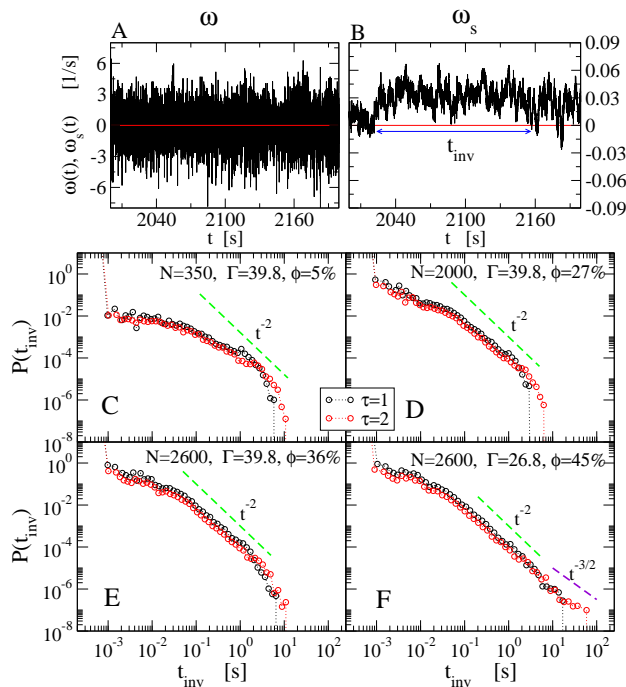


FIG. 4: A and B: angular velocity $\omega(t)$ and filtered signal $\omega_s(t)$ (with a running average over a time $\tau = 2$ s), for $N = 2600$ and $\Gamma = 26.8$. C,D,E,F: pdf of the inversion times calculated (with $\tau = 1$ s and $\tau = 2$ s) in different experiments. From C to F the following configurations are displayed: very dilute, intermediate, dense at high energy, dense at low energy. Colored dashed lines are guides for the eye.

monic potential with “stiffness” K and unfixed minimum, under the effect of a thermal bath at temperature T and relaxation time I/γ . The harmonic potential, representing the cage due to the confining effect of the dense granular host fluid, is not fixed but moves, as $\theta_0(t)$ behaves as Brownian motion with diffusivity D_0 . Motivation for this model is twofold: 1) the main features of the vpds, i.e. an elastic resonance (region III) and a plateau revealing loss of memory at larger times (region II); 2) in the dilute limit it can be rigorously derived [28], while at intermediate densities a series of studies showed that memory effects (coming from correlated collisions) are well described by a coupling with an additional degree of freedom fluctuating at slower time-scales [23]. The vpds of the above model can be calculated and reads

$$S(f) = \frac{1}{\pi} \frac{D_0 K^2 + \gamma T (2\pi f)^2}{\gamma^2 (2\pi f)^2 + [K - I(2\pi f)^2]^2}. \quad (2)$$

Two limiting cases are recovered: when $K = 0$, the Ornstein-Uhlenbeck process is obtained, with $S(f)$ taking the Lorentzian form mentioned before. When $K > 0$ and $D_0 = 0$, one has the Klein-Kramers process in a fixed harmonic potential, and $S(f) \rightarrow 0$ for $f \rightarrow 0$, expressing the absence of diffusion at large times: the cage does not move and fully confines the particle. Formula (2) fairly fits all experimental spectra in regions II and III, with pa-

rameters given in Tables 2 and 3 of [21]. Reasonably, the “cage stiffness” decreases at increasing shaking intensity. It also decreases as the density is reduced, and abruptly goes to zero for $N \sim 1000$. The “cage diffusivity” D_0 rapidly increases with increasing Γ and with decreasing N . A more detailed study of the transition from the cage behavior $K \neq 0$ to the free behavior $K = 0$ is postponed to future investigations.

A more ambitious task is to devise a simple mechanism for $\omega_s(t)$, leading to superdiffusion. In driven granular systems it has been observed below the jamming transition [12] and in a few cases above it, where it was imputed to “zero”-modes of the host fluid [10], to Taylor dispersion [13], or to turbulence-like cascade effects [29]. We stress that, at variance with standard diffusion, for anomalous diffusion there is nothing similar to universality [30]. A systematic derivation of anomalous diffusion is a hard task and it is possible only in few specific cases [30]. Of course, the basic ingredient must be an enduring memory: a way to achieve it is to replace standard time derivatives with fractional derivatives in the Fokker-Planck equations, an approach which is subject of a vast literature [31]. Such an approach is capable, in principle, of describing both caging and superdiffusion within a single model equation, at the price of losing immediate interpretation and plain calculations. In a complementary approach [32] a coarse-grained value of $\omega_s(t)$ (where only the sign of this quantity is traced) follows a continuous time random walk (ctrw): It takes discrete values with random transition times extracted from a given distribution. A simplified version of the ctrw is discussed in the SM [21]. We highlight that the ctrw gets a suggestive experimental confirmation in the observations of Fig. 4: indeed the ctrw model quantitatively connects the observed slow decay of $P(t_{inv})$ to superdiffusion.

Conclusion: an experimental study of dense granular mesorheology allows to probe time-scales in a range of six orders of magnitude. Such an investigation reveals a complex scenario with different dynamical behaviors in four frequency or time regions. Three crucial features are observed at large density and low temperature: a “resonant” caging phenomenon at intermediate scales, non-white noise at fast scales, and super-diffusion at long times. The caging phenomenon is compatible with a diffusing harmonic cage model, while superdiffusion seems to be rooted in the long inversion times appearing in the dynamics $\omega_s(t)$, possibly related to creeping rotating motion of the granular media. A more detailed investigation of *transitions* is in order: a gas-liquid transition could be put in evidence by studying how $K \rightarrow 0$ when N decreases; a liquid-glass transition could be taking place at the lowest values of Γ or, eventually increasing $N > 2600$. Superdiffusion and large values of t_{inv} could be signaling such a transition. Another promising line of investigation is *active* mesorheology, i.e. probing the response of the system to the application of an external force, achieved

by coupling a controllable motor to the blade [19].

We wish to thank A. Lasanta Becerra and A. Sarracino for useful discussions. AP acknowledges the support of the Italian MIUR grants FIRB-IDEAS n. RBID08Z9JE.

-
- [1] B. Andreotti, Y. Forterre and O. Pouliquen, *Granular Media. Between Fluid and Solid.*, Cambridge University Press (2013).
- [2] R. A. Bagnold, Proc. Royal Soc. London **225**, 49 (1954).
- [3] G. H. Wortel, J. A. Dijksman, and M. van Hecke, Phys. Rev. E **89**, 012202 (2014).
- [4] P. Wang, C. Song and H. A. Makse, Nat. Phys. **2**, 526 (2006).
- [5] C. Song, P. Wang and H. A. Makse, Proc. Nat. Acad. Sci **102**, 2299 (2005).
- [6] M. van Hecke, J. Phys.: Condens. Matter **22**, 033101 (2010).
- [7] G. D’Anna, P. Mayor, A. Barrat, V. Loreto and F. Nori, Nature **424**, 909 (2003).
- [8] N. V. Brilliantov and T. Pöschel, *Kinetic Theory of Granular Gases*, Oxford University Press (2004).
- [9] J. C. Dyre, Rev. Mod. Phys. **78**, 953 (2006).
- [10] C. Heussinger, L. Berthier and J.-L. Barrat, Europhys. Lett. **90**, 20005 (2010).
- [11] L. Cipelletti, S. Manley, R. C. Ball, and D. A. Weitz, Phys. Rev. Lett. **84**, 2275 (2000).
- [12] F. Lechenault, O. Dauchot, G. Biroli and J. P. Bouchaud, Europhys. Lett. **83**, 46003 (2008).
- [13] B. Utter and R. P. Behringer, Phys. Rev. E **69**, 031308 (2004).
- [14] D. M. Mueth, G. F. Debregeas, G. S. Karczmar, P. J. Eng, S. R. Nagel and H. M. Jaeger, Nature **406**, 385 (2000).
- [15] J. Brujić, C. Song, P. Wang, C. Briscoe, G. Marty, and H. A. Makse, Phys. Rev. Lett. **98**, 248001 (2007).
- [16] T. M. Squires and T. G. Mason, Annu. Rev. Fluid. Mech. **42**, 413 (2010).
- [17] G. Marty and O. Dauchot, Phys. Rev. Lett. **94**, 015701 (2005).
- [18] A. L. Sellerio, D. Mari, G. Gremaud, and G. D’Anna, Phys. Rev. E **83**, 021301 (2011).
- [19] A. Gnoli, A. Puglisi, A. Sarracino and A. Vulpiani, Plos One **9**, e93720 (2014).
- [20] A. Naert, Europhys. Lett. **97** 20010 (2012).
- [21] See Supplemental Material at [URL will be inserted by publisher] for details on experimental setup, theory and simulations.
- [22] M. B. Weissman, Rev. Mod. Phys. **60**, 537 (1988).
- [23] A. Sarracino, D. Villamaina, G. Gradenigo, A. Puglisi, Europhys. Lett. **92**, 34001 (2010).
- [24] P. M. Reis, R. A. Ingale, and M. D. Shattuck, Phys. Rev. Lett. **98**, 188301 (2007).
- [25] A. Fiege, T. Aspelmeier, and A. Zippelius, Phys. Rev. Lett. **102**, 098001 (2009).
- [26] V. F. Sears, Proc. Phys. Soc. **86**, 953 (1965).
- [27] W. Coffey, Yu. P. Kalmykov and J. T. Waldron, *The Langevin Equation: With Applications in Physics, Chemistry, and Electrical Engineering*, World Scientific (Singapore, 1996)
- [28] A. Sarracino, D. Villamaina, G. Costantini and A. Puglisi, J. Stat. Mech. P04013 (2010).
- [29] F. Radjai and S. Roux, Phys. Rev. Lett. **89**, 064302 (2002).
- [30] R. Klages, G. Radons and I. M. Sokolov (eds.), *Anomalous transport*, Wiley&Sons (2008).
- [31] J. Klafter, S. C. Lim and R. Metzler (eds.), *Fractional Dynamics: Recent Advances*, World Scientific (Singapore, 2012).
- [32] K.H. Andersen, P. Castiglione, A. Mazzino and A. Vulpiani, Eur. Phys. J. B **18**, 447 (2000).

SM: SUPPLEMENTAL MATERIAL

DETAILS OF THE EXPERIMENTAL SETUP

The scheme of our experimental setup is shown in Fig. 1A. A Poly(methyl methacrylate) (PMMA) container (diameter 90 mm, maximum height 47 mm and total volume 245 cm³) with an inverse-conical-shaped base, is filled with N steel spheres (diameter 4 mm) and mounted on an electrodynamic shaker (LDS V450) which is fed, through an amplifier, with a noisy signal whose spectrum is approximately flat in a range $[f_{min}, f_{max}]$ with $f_{min} = 200$ Hz and $f_{max} = 400$ Hz. The shaker responds roughly linearly in the same range of frequencies, as verified with an accelerometer placed on the container. The elevation of the container at time t is denoted by $z(t)$. We give the range of values for the relevant variables: for the maximum acceleration $\ddot{z}_{max} \sim 20 - 40$ g, the maximum velocity $\dot{z}_{max} \sim 80 - 300$ mm/s and the maximum displacement $z_{max} \sim 0.03 - 0.25$ mm. Details are reported below in Table 1. A PMMA blade (dimensions $35 \times 6 \times 15$ mm, momentum of inertia $I = 353$ g·mm²), suspended to a mounting which is mechanically isolated from the container/shaker apparatus, is immersed into the granular medium and can rotate around a vertical axis placed at the center of the container. The angular velocity $\omega(t)$ of the blade and its absolute (i.e. without the modulus 2π operation) angle of rotation $\theta(t) = \int_0^t \omega(t') dt'$ are measured by an angular encoder (AEDA-3300) at a time-resolution of 2 kHz and angular resolution 40000 divisions per revolution. The granular medium is in a liquid state because of the vibration. The blade, under the effect of the interactions with the spheres, performs a motion qualitatively similar to an angular Brownian motion. It is important to remark that the blade can only rotate and therefore moves along the “free flow” direction, i.e. it only probes the fluctuations of granular modes parallel to the boundaries of the container. Moreover, the blade’s size is such that, in the dense cases, its rotation is only allowed by the rearrangement of a large number of surrounding particles. We have performed two families of experiments: experiments at high density ($N = 2600$) and different normalized (i.e. in g units) shaking intensities $\Gamma = \ddot{z}_{max}/g \in [19.5, 39.8]$, and experiments at high shaking intensity ($\Gamma = 39.8$) and different densities $N \in [300, 2600]$. In Fig. 1B and C we have reported the values of the mean squared angular velocity $\langle \omega^2 \rangle$ of the blade in the different experiments.

Γ	39.8	35.2	30.6	26.8	23	19.5
$z_{min} - z_{max}$	0.25-0.06	0.22-0.05	0.19-0.05	0.17-0.04	0.14-0.04	0.12-0.03
$\dot{z}_{min} - \dot{z}_{max}$	310.4-155.2	274.5-137.3	238.6-119.3	209-105	179.4-89.7	152-76

TABLE I: Equivalence between the normalized shaking intensity Γ and the physical amplitudes and velocities of the container, expressed in mm and mm.s⁻¹, with $f_{min} = 200$ Hz and $f_{max} = 400$ Hz

FITS OF THE EXPERIMENTAL DATA: PARAMETERS

Γ	D_0	$K/[I(2\pi)^2]$	γ/I	T/I	$\frac{T/I}{\langle \omega^2 \rangle}$	T/γ
g	$10^{-5} s^{-1}$	s^{-2}	s^{-1}	s^{-2}		s^{-1}
39.8	46 ± 4	128 ± 3	121 ± 3	0.51 ± 0.01	0.54	0.0042
35.2	31 ± 3	151 ± 4	134 ± 4	0.47 ± 0.01	0.53	0.0035
30.6	13 ± 2	181 ± 4	151 ± 4	0.371 ± 0.009	0.51	0.0024
26.8	8 ± 1	215 ± 5	171 ± 5	0.307 ± 0.007	0.5	0.0018
23	4.6 ± 0.8	260 ± 7	217 ± 7	0.241 ± 0.006	0.47	0.0011
19.5	2.6 ± 0.5	320 ± 7	250 ± 7	0.198 ± 0.005	0.44	0.00079

TABLE II: Fit’s parameters with Eq. 2, series $N = 2600$ and $\Gamma \in [19.5, 39.8]$.

N	D_0 10^{-3} s^{-1}	$K/[I(2\pi)^2]$ s^{-2}	γ/I s^{-1}	T/I s^{-2}	$\frac{T/I}{\langle \omega^2 \rangle}$	T/γ s^{-1}
2600	0.46 ± 0.04	128 ± 3	121 ± 3	0.51 ± 0.01	0.54	0.0042
2000	1.44 ± 0.04	88 ± 2	103 ± 2	0.57 ± 0.02	0.52	0.0055
1300	7.7 ± 0.1	84 ± 18	131 ± 6	0.97 ± 0.08	0.54	0.0074
700 (gas)	0	0	102 ± 9	$7.0 \pm 1.$	1.1	0.069
350 (gas)	0	0	79 ± 16	$16.0 \pm 2.$	1.1	0.2

TABLE III: Fit's parameters with Eq. 2, series $\Gamma = 39.8 \text{ g}$ and $N \in [350, 2600]$.

EXPERIMENTS WITH BLADES OF DIFFERENT SIZES

We have performed a number of experiments with different blades, changing the total scattering surface and its shape. The thickness of the blades being constant, as well as its material, the mass and momentum of inertia are also varied accordingly.

In Figure 5a we portray the four shapes used. Shape ‘‘A’’ is the one used in the rest of the paper. Panels *b* and *c* of Figure 5 represent the vpds and the msd respectively, with the four shapes, in the case with $\Gamma = 30.6$ and $N = 2600$, corresponding to packing fraction $\phi = 40\%$. It appears that the general features of the vpds and msd are conserved when the size and shape of the blade are changed. Higher or smaller energy is obviously observed, when the inertia is reduced (shapes C and D) or increased (shape B). Differences in the mechanical (spurious) resonance at $\sim 70 - 100$ Hz are due to some modifications of the mounting mechanism on which the blade is fixed, occurred between the old and the new experiments. In the msd of the larger blade (shape B) it is observed - at large times - a saturation of the mean squared displacement which we impute to border effects. Note also that at very large time the measurement of the msd is noisy and prone to errors.

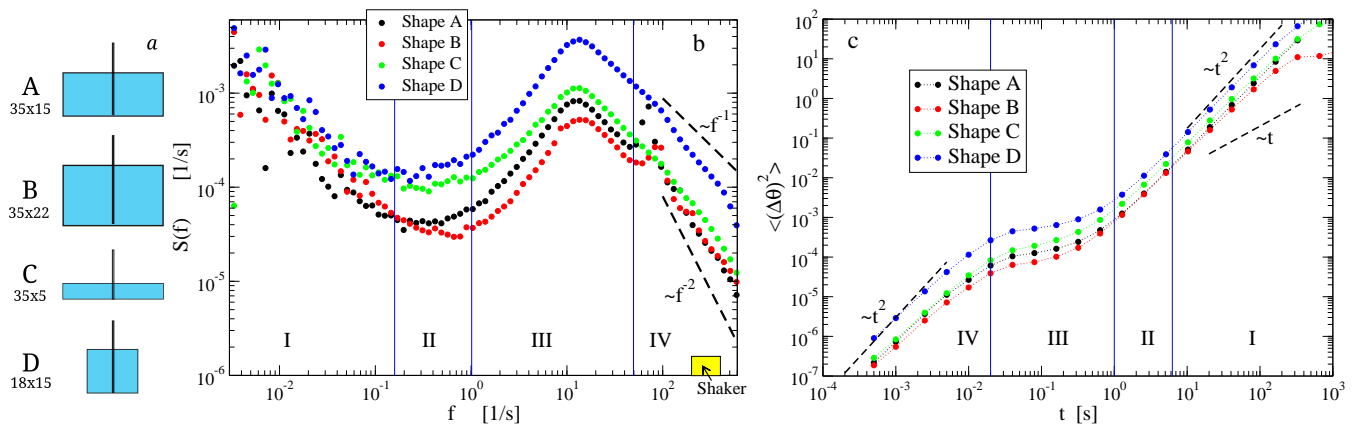


FIG. 5: Effect of the size and shape of the blade. The four shapes are represented in panel *a*. In panel *b* we show the velocity power density spectrum for the four cases, with $\Gamma = 30.6$ and $N = 2600$ which corresponds to packing fraction $\phi = 40\%$. For the same parameters, the behavior of the mean squared displacement is displayed in panel *c*.

VERY LONG EXPERIMENTS

The finite size of the experiment suggests that all relaxation times, even if long, are finite: the displacement $\Delta\theta$, therefore, is expected to reach asymptotically a normal diffusive behavior. We have performed a 12-hours-long experiment in order to check such a hypothesis. The mean squared displacement is shown in Fig. 6. Indeed, at large times the superdiffusive behavior shows a crossover toward normal diffusion, which is slowly approached after many hours.

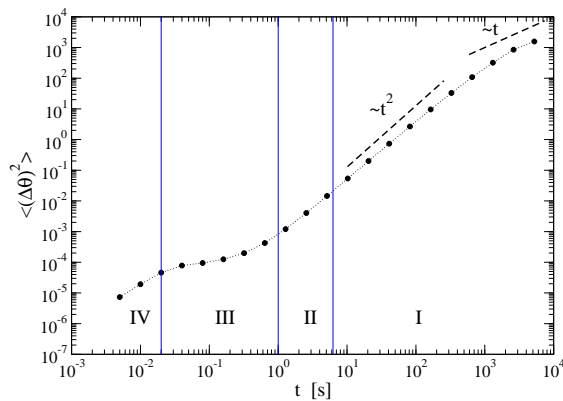


FIG. 6: Mean squared displacement in a long experiment (total time 12 hours), with $N = 2600$ and $\Gamma = 26.8$.

THE CONTINUOUS TIME RANDOM WALK MODEL

A possible mechanism for superdiffusion is the *continuous time random walk* model (ctrw) [30, 32]. In the ctrw the variable (here the velocity) performs a random walk taking discrete values ω_i : it remains constant for a random time t and then jumps to a new value. The choice of the statistics (pdf) of t is the main parameter of the model and determines the properties of the autocorrelation of the velocity and, therefore, of the mean squared displacement.

Here we consider in details a simplified version of the ctrw model, where the velocity can take only two values. Such a simplification does not change the substance of the demonstration, which can be easily generalised to models with many possible values. Note that a comparison between this model and the experimental results should be made only at long time scales (i.e. such that $\Delta\theta(t)$ is well approximated by $\int_0^t \omega_s(s) ds$) and in the spirit of a strong coarse-graining, as if a dramatic loss of resolution allows to measure only the sign of the velocity.

In the model, ω_s changes its value at times t_n with $n \in [0, m]$ and $t_m = t$. In the interval between t_{n-1} and t_n , ω_s takes the value $\omega_{0,n} \in [-\omega_0, \omega_0]$. The intervals $t_{inv,n} = t_n - t_{n-1}$, with $\sum_1^m t_{inv,n} = t$, are random and independent with the following probability density function

$$P(t_{inv} = x) \sim \begin{cases} g(x) & x \in [0, t^*] \\ x^{-g} & x \in (t^*, t_{max}] \\ 0 & x > t_{max}. \end{cases} \quad (3)$$

where $g(x)$ is a smooth function: its shape and the value of t^* (assumed to be always finite) are not relevant for the long time behavior of the displacement. The cut-off t_{max} may eventually be taken to ∞ (see below).

For the msd therefore we have

$$\langle [\Delta\theta(t)]^2 \rangle = \left\langle \left[\int_0^t \omega_s(s) ds \right]^2 \right\rangle = \omega_0^2 \sum_{n=1}^m \langle t_{inv,n}^2 \rangle + \sum_{n \neq k} \langle \omega_{0,n} \omega_{0,k} \rangle \langle t_{inv,n} t_{inv,k} \rangle \quad (4)$$

and the values $\omega_{0,n}$ being independent and with zero average, one may drop the last term obtaining

$$\langle [\Delta\theta(t)]^2 \rangle = \omega_0^2 \sum_1^m \langle t_{inv,n}^2 \rangle = m \omega_0^2 \langle t_{inv,n}^2 \rangle \quad (5)$$

The presence of the cut-off allows us to write

$$\langle t_{inv} \rangle = \frac{t}{m}. \quad (6)$$

and therefore one finally has

$$\langle [\Delta\theta(t)]^2 \rangle = \omega_0^2 \frac{\langle t_{inv}^2 \rangle}{\langle t_{inv} \rangle} t. \quad (7)$$

The dependence on the cut-off (at large values of t_{max}) of the moments of order $k \geq 1$ of $P(t_{inv})$ are determined by the distribution at times larger than t^* , i.e.

$$\lim_{t_{max} \rightarrow \infty} \langle t_{inv}^k \rangle \sim \lim_{t_{max} \rightarrow \infty} \int_{t^*}^{t_{max}} x^{k-g} dx \sim \begin{cases} \text{const.} & g > k + 1 \\ t_{max}^{k+1-g} & g \leq k + 1, \end{cases} \quad (8)$$

The last equality, together with Eq. (7), gives three possible behaviors for the msd at large times $t \gtrsim t_{max}$:

- for $g > 3$: normal diffusion, independently of the cut-off t_{max} ;
- for $2 < g \leq 3$: $\langle [\Delta\theta(t)]^2 \rangle \sim t_{max}^{3-g} t$;
- for $1 < g \leq 2$: $\langle [\Delta\theta(t)]^2 \rangle \sim t_{max} t$.

For $1 < g \leq 3$, in the range $t \leq t_{max}$, one expects $\langle [\Delta\theta(t)]^2 \rangle \sim t^\beta$. The value of β can be determined by asking that it matches, at $t \sim t_{max}$, the asymptotic behavior given above: for instance in the case $2 < g \leq 3$ the behaviors $\langle [\Delta\theta(t)]^2 \rangle \sim t_{max}^{3-g} t$ and $\langle [\Delta\theta(t)]^2 \rangle \sim t^\beta$ can match only if $\beta = 4 - g$; the same argument for $1 < g \leq 2$ gives $\beta = 2$. The situation is therefore summarized here

$$\langle [\Delta\theta(t)]^2 \rangle \sim \begin{cases} t & g > 3 \text{ or } t \gtrsim t_{max} \\ t^{4-g} & 2 < g \leq 3 \text{ and } t < t_{max} \\ t^2 & 1 < g \leq 2 \text{ and } t < t_{max}. \end{cases} \quad (9)$$

Fig. 4 of the Letter shows that $P(t_{inv})$ has an exponential cut-off at $t_{max} \lesssim 10$ seconds for all the experiments where diffusive behavior is observed, that is in the most dilute or energetic cases. The cut-off rapidly grows and reaches times of the order of the duration of the experiment when $N = 2600$ and $\Gamma < 31$: a power law tail with $g \lesssim 2$ emerges. Equation (9) makes this power law decay fully consistent with the ballistic behavior observed in Fig. 3 of the Letter.